Energy & Environmental Science

RSC Publishing

PAPER

View Article Online
View Journal | View Issue

Cite this: *Energy Environ. Sci.*, 2013, **6**, 2529

Improving the long-term stability of PBDTTPD polymer solar cells through material purification aimed at removing organic impurities†

William R. Mateker,[a] Jessica D. Douglas,[b] Clément Cabanetos,[c] I. T. Sachs-Quintana,[a] Jonathan A. Bartelt,[a] Eric T. Hoke,[d] Abdulrahman El Labban,[c] Pierre M. Beaujuge,[c] Jean M. J. Fréchet[bc] and Michael D. McGehee*[a]

Received 19th April 2013
Accepted 17th June 2013

DOI: 10.1039/c3ee41328d

www.rsc.org/ees

While bulk heterojunction (BHJ) solar cells fabricated from high M_n PBDTTPD achieve power conversion efficiencies (PCE) as high as 7.3%, the short-circuit current density (J_{SC}) of these devices can drop by 20% after seven days of storage in the dark and under inert conditions. This degradation is characterized by the appearance of S-shape features in the reverse bias region of current–voltage (*J–V*) curves that increase in amplitude over time. Conversely, BHJ solar cells fabricated from low M_n PBDTTPD do not develop S-shaped *J–V* curves. However, S-shapes identical to those observed in high M_n PBDTTPD solar cells can be induced in low M_n devices through intentional contamination with the TPD monomer. Furthermore, when high M_n PBDTTPD is purified *via* size exclusion chromatography (SEC) to reduce the content of low molecular weight species, the J_{SC} of polymer devices is significantly more stable over time. After 111 days of storage in the dark under inert conditions, the *J–V* curves do not develop S-shapes and the J_{SC} degrades by only 6%. The S-shape degradation feature, symptomatic of low device lifetimes, appears to be linked to the presence of low molecular weight contaminants, which may be trapped within samples of high M_n polymer that have not been purified by SEC. Although these impurities do not affect initial device PCE, they significantly reduce device lifetime, and solar cell stability is improved by increasing the purity of the polymer materials.

Broader context

Organic photovoltaics (OPV) has emerged as a promising technology for energy production, with distinct advantages in processing and manufacturing over inorganic technologies. Single junction efficiencies have improved rapidly and tandem solar cells have demonstrated efficiencies exceeding 10%. In addition to a high efficiency, OPV devices must demonstrate lifetimes approaching those of inorganic materials. Long-term OPV stability can vary between different materials. Additionally, device stability often varies across different batches of one single material. Such batch-to-batch variance implicates impurities, though the exact role impurities play in OPV lifetime is unknown. In solar cells made from a high efficiency polymer, we observe that batches with high molecular weight (M_w) show rapid device degradation while batches with low M_w show longer device lifetimes. We link the degradation behavior of high M_w batches to organic impurities structurally similar to the polymer. Finally, we show that increased purification of high molecular weight batches can dramatically improve device lifetime. We suspect that batch-to-batch variance can be decreased in polymer OPV through stricter purification protocol.

Introduction

Solution-processed organic photovoltaics (OPVs), based on bulk heterojunction (BHJ) blends of semiconducting polymers and fullerene derivatives,[1] offer a pathway to low-cost, lightweight, and flexible solar cells.[2] The development of donor–acceptor (D–A) copolymers has allowed for synthetic manipulation of polymer energy levels, enhancing both light absorption and voltage generation in BHJ devices.[3–5] These improvements have enabled single junction polymer–fullerene devices to obtain power conversion efficiencies (PCEs) above 8%.[6–10] Such high efficiencies have increased interest in the operating lifetimes of OPVs.[11,12] Lifetimes exceeding 6 years have been reported for glass-on-glass encapsulated, solution-processed BHJ OPVs based on the polymer PCDTBT blended with the fullerene derivative [6,6]-phenyl-C_{71}-butyric acid methyl ester ($PC_{71}BM$).[13]

External stresses are known to influence the operating lifetime of BHJ devices. Operating temperatures of solar cells in the field can reach 35 °C above ambient.[14] Previous work has

[a]*Department of Materials Science and Engineering, Stanford University, Stanford, CA 94305, USA. E-mail: mmcgehee@stanford.edu*

[b]*Department of Chemistry, University of California, Berkeley, CA 94720, USA*

[c]*King Abdullah University of Science and Technology (KAUST), Thuwal, 23955-6900, Saudi Arabia*

[d]*Department of Applied Physics, Stanford University, Stanford, CA 94305, USA*

† Electronic supplementary information (ESI) available. See DOI: 10.1039/c3ee41328d

examined the changes in some BHJ blend morphologies in response to temperatures within the range of expected operating conditions.[15,16] Polymers with glass transition temperatures above operating conditions[17–19] and crosslinkable polymers[20,21] have demonstrated improved thermal stability, even at temperatures higher than a solar cell would likely experience during operation. Degradation of the active layer materials in the presence of light and atmosphere has also been widely investigated, as conjugated polymers are sensitive to photooxidation.[22–27] To further the design of stable BHJ components, the relative photooxidation rates of common monomers used in D–A copolymers have been reported,[28] as well as the role of fullerene derivatives as either antioxidants or prooxidants in BHJ blends exposed to light and atmosphere.[29]

While much has been reported about the effects of heat, light, and atmosphere on OPV lifetime, less is known about the role of impurities. Impurities can be introduced into the active layer materials at different stages of material preparation and OPV device fabrication. For example, it has been shown that silicone and siloxane impurities extrinsically introduced into the blend solutions from plastic syringes affect the BHJ morphology and can either improve or diminish initial device performance.[30,31] Additionally, palladium-, tin-, and halogen-containing impurities can remain within polymer samples that were synthesized *via* high-yielding Stille cross-coupling reactions,[32–35] despite thorough purification protocols.[36–38] These metals and halogen impurities have been shown to be detrimental to the initial performance and the lifetime of other organic electronic devices, such as OLEDS and transistors.[39–41]

In addition to metal-based contaminants, low molecular weight organics, such as unreacted or deactivated monomers, degradation products, cross-coupling byproducts, and low molecular weight oligomers, may remain within the polymer.[35] Solar cells based on solution-processed small-molecule donors have also achieved efficiencies exceeding 8%,[42,43] and recently, solar cell devices based on the small-molecule donor *p*-DTS(PTTh$_2$)$_2$ were found to be hindered by a Stille cross-coupling byproduct. Even with byproduct concentrations of less than 1%, the initial performance of *p*-DTS(PTTh$_2$)$_2$:PC$_{71}$BM devices was significantly reduced.[44] In polymeric materials, low molecular weight chains and oligomers result from the relatively broad molecular weight distributions (PDI typically > 1.5) obtained with step-growth polymerizations. It has also been shown that mismatching the D–A comonomer ratio during Stille polymerization can increase the molecular weight of low band-gap copolymers.[45] This approach may contribute to increased concentrations of unreacted organic impurities within the polymer, with possible implications for OPV device stability.

In this work, we investigate the role of organic contaminants on the stability of BHJ solar cells fabricated from a blend of poly(di(2-ethylhexyloxy)benzo[1,2-*b*:4,5-*b*′]dithiophene-*co*-octylthieno[3,4-*c*]pyrrole-4,6-dione) (PBDTTPD)[46–48] and PC$_{61}$BM. While BHJ solar cells fabricated from high M_n PBDTTPD initially outperform those prepared with low M_n PBDTTPD devices, we show that high M_n PBDTTPD solar cells suffer from a characteristic loss of short-circuit current density (J_{SC}) after storage under dark, inert conditions (glovebox environment). We observe that the loss of J_{SC} in high M_n PBDTTPD solar cells is caused by an S-shape in the reverse bias region of the current–voltage (J–V) curve, which increases in severity over time. We also show that BHJ solar cells, similarly fabricated from low M_n PBDTTPD and subjected to the same storage conditions, do not suffer from the S-shape degradation feature. However, when solutions of low M_n PBDTTPD are intentionally contaminated with a low molecular weight organic impurity, specifically the TPD monomer, we observe an S-shape degradation feature that is identical to that observed in high M_n PBDTTPD devices. Thus, we link this characteristic degradation feature to the presence of low molecular weight contaminants within high M_n PBDTTPD samples.

In parallel, solar cells fabricated from a batch of extensively purified high M_n PBDTTPD show minimal loss of J_{SC} after 111 days of glovebox storage and no S-shapes in the reverse bias region of their J–V curves. Material purification is achieved *via* fractionation of this high M_n polymer by preparative size exclusion chromatography (SEC), a protocol by which some of the low molecular weight organic species is separated from longer polymer chains. Although low molecular weight organics do not significantly affect the initial PCE of PBDTTPD solar cells, we show that extensive polymer purification, aimed at reducing the content of organic small molecules, leads to solar cells with improved storage lifetimes.

Results and discussion

Initial solar cell performance

BHJ solar cells were fabricated from five separate batches of PBDTTPD over the course of this study. Two batches were synthesized with low M_n (26 kDa), while another three were synthezied with high M_n (35–41 kDa) (Fig. 1). Low M_n PBDTTPD devices obtained a maximum PCE of 5.3% when blended in a 1 : 1.5 weight ratio with PC$_{61}$BM (Fig. 2). In contrast, solar cells fabricated from all three high M_n PBDTTPD batches showed PCEs as high as 7.3% in a 1 : 1.5 weight ratio blend with PC$_{61}$BM (Fig. 2). Both the J_{SC} ($\sim$11 mA cm^{-2}) and fill factor (FF) ($\sim$0.70) of high M_n PBDTTPD devices were greater than those of their low M_n counterparts, while the open-circuit voltage (V_{OC}) (0.95 V) appeared to be unaffected by polymer molecular weight. A full discussion on the effect of molecular weight on initial PCE is beyond the scope of this paper and will be the subject of a separate study. The present work focuses on the difference in device degradation between high and low M_n PBDTTPD.

PBDTTPD solar cell degradation

During degradation studies, solar cells were stored and tested under inert atmosphere (glovebox environment), in the dark, and at room temperature. In total, 766 solar cells, on 152 different substrates, were fabricated from all three batches of high M_n PBDTTPD and monitored periodically. The observed degradation of BHJ solar cells fabricated from all three high M_n polymer batches followed the same pattern; furthermore, the degradation pattern was highly reproducible across all three high M_n PBDTTPD batches. This pattern was observed to be

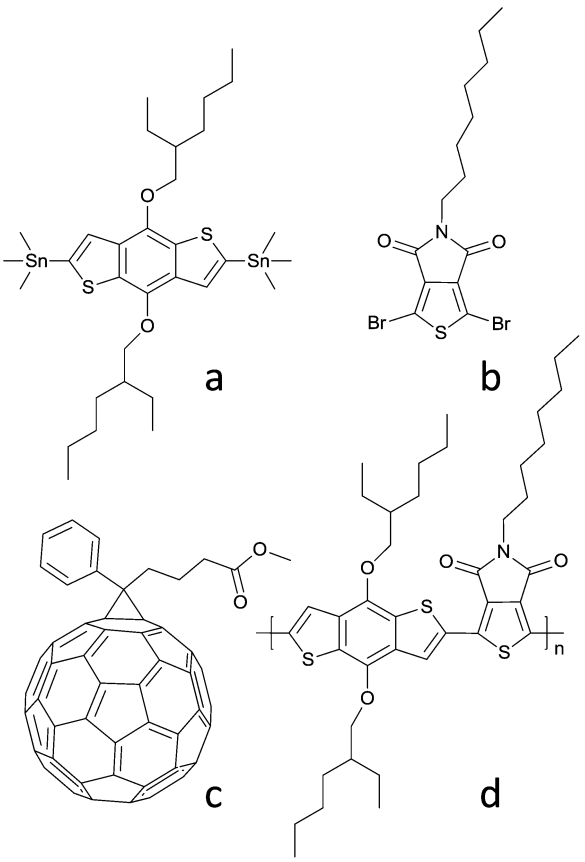

Fig. 1 The chemical structures of (a) the BDT and (b) TPD monomers, (c) the fullerene derivative $PC_{61}BM$, and (d) the PBDTTPD polymer.

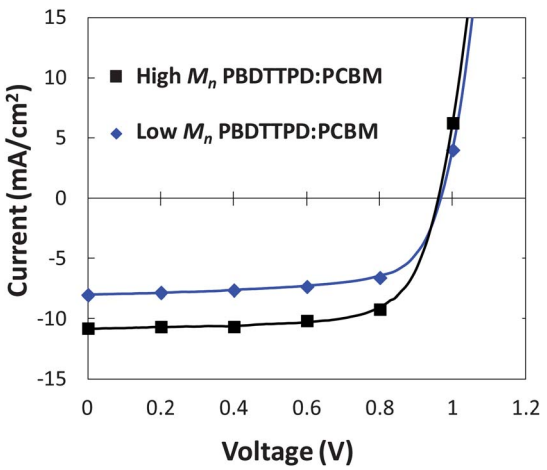

Fig. 2 *J–V* curves of representative PBDTTPD:$PC_{61}BM$ BHJ solar cells. Devices fabricated from high M_n (Batch #H2) PBDTTPD produce greater J_{SC}, fill factor, and PCE values than low M_n polymer devices.

independent of processing conditions, device fabricators, and fullerene type ($PC_{61}BM$ *vs.* $PC_{71}BM$) or source (NanoC *vs.* Solenne). To quantitatively assess the device degradation pattern, 56 BHJ solar cells on 12 substrates, all fabricated simultaneously from a blend of 37 kDa PBDTTPD and NanoC $PC_{61}BM$, were subjected to daily *J–V* testing over 28 days of glovebox storage (Fig. 3). Following 7 days of storage, the average PCE decreased by 25% (Fig. 3a), mainly as a result of a significant drop in J_{SC} (Fig. 3b). In contrast, the device V_{OC} remained stable (Fig. 3c) and the FF decreased by less than 10% (Fig. 3d) over the full 28 days of testing. Despite observing a large range in degradation between devices, all of the fabricated solar cells suffered at least a 10% drop in initial PCE over the course of the aging experiment. Table S1† summarizes the device degradation data for this experiment.

After only a few days of storage, an S-shape feature developed in the *J–V* curves of all the high M_n PBDTTPD devices (Fig. 4a). This S-shape appeared at a reverse bias of approximately −1.25 V and the severity increased as the devices aged. At reverse biases exceeding −2 V, the device photocurrent converged to the initial photocurrent, indicating that S-shape formation was the dominant degradation feature and the source of J_{SC} loss in initially high-performing, high M_n PBDTTPD:$PC_{61}BM$ solar cells. This degradation feature was inherent to the high M_n PBDTTPD – no other polymer systems tested in our laboratory, such as PCDTBT, PBTTT, MDMO-PPV, P3HT, or PBDTTT-C-T, showed S-shapes in the reverse bias region of *J–V* curves that grew with time under the same glovebox storage conditions. The severity of the S-shape varied among substrates, as well as across devices on the same substrate, leading to a large range of J_{SC} loss across devices (Fig. 3b). Normalizing the J_{SC} degradation for each substrate revealed that the severity of degradation often extended radially from a single device, so that devices towards the edge of any substrate were typically the most degraded (Fig. S2†).

Our low M_n devices showed improved shelf stability relative to the degradation observed in high M_n PBDTTPD solar cells. After 26 days of storage in inert conditions, 35 BHJ solar cells suffered only a 14% drop in both J_{SC} and PCE. More importantly, none of the 65 solar cells on 13 different substrates, fabricated from two different low M_n PBDTTPD polymers, developed an S-shape degradation feature in the reverse bias region (see ESI,† Section 2). These observations were consistent with previous reports on PBDTTPD shelf stability.[49]

The existence of S-shape features in the *J–V* curves of illuminated devices has been attributed to several mechanisms.[50–55] For example, S-shape features have been reproduced in model simulations of BHJ solar cells by introducing surface dipoles,[56] energy barriers,[57] and charge accumulation at the interfaces between the active layer and the electrodes.[58] The location of a S-shape feature in the reverse bias region suggests that an extraction barrier forms at one of the electrodes and prevents efficient charge collection. In high M_n PBDTTPD devices, we propose that such an extraction barrier is not initially present, but forms over time at one of the electrodes. Assuming that an extraction barrier causes S-shape features to form, the replacement of either the cathode or anode should reinstate a flat photocurrent throughout the reverse bias region.

In order to probe this assumption, the cathode of a degraded, high M_n PBDTTPD:$PC_{61}BM$ device was removed with Scotch tape,[59,60] and a new electrode (Ca/Al) was vapor-deposited

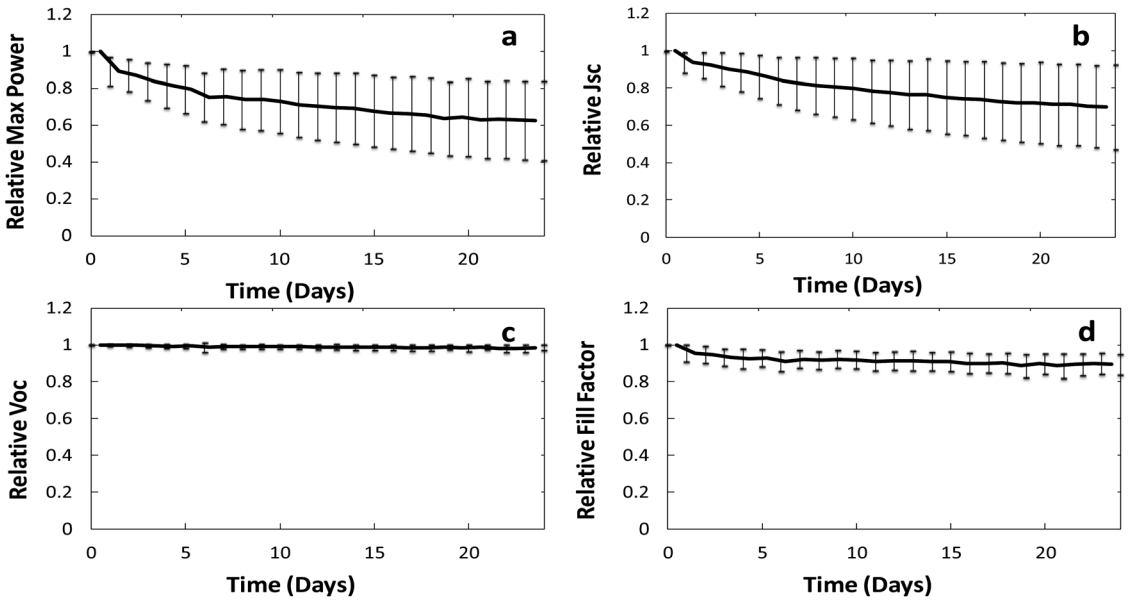

Fig. 3 Degradation curves for high M_n (Batch #H2) PBDTTPD:$PC_{61}BM$ solar cells aged over 28 days. The error bars represent the standard deviation among devices. (a) The relative device PCE decreases to about 60% of the initial value. (b) The relative J_{SC} drops to about 70% of its initial value. There is a large range in the observed degradation between devices. (c) The relative V_{OC} is stable over the course of the experiment. (d) The relative FF drops by only about 10% over four weeks of storage in the glovebox. As PCE = $J_{SC} \times V_{OC} \times$ FF, the observed decrease in PCE is dominated by the degradation of the J_{SC}.

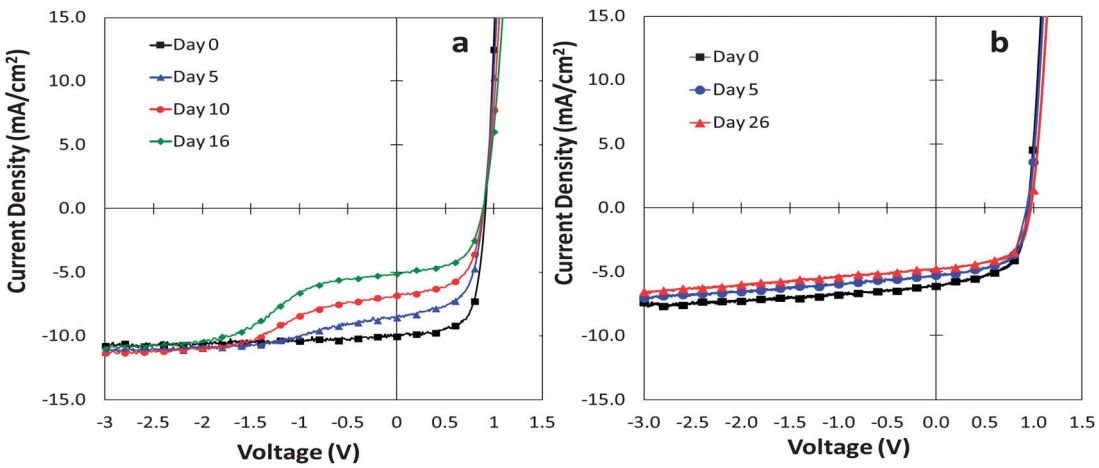

Fig. 4 (a) The *J–V* curves of a representative high M_n (Batch #H2) PBDTTPD:$PC_{61}BM$ solar cell aged over 16 days in a glovebox. At day 0, the photocurrent in the reverse bias region is flat. By day 5, an S-shape feature develops in the reverse bias region, and continues to develop with time. (b) A representative low M_n PBDTTPD:$PC_{61}BM$ solar cell does not develop the S-shaped degradation feature over a longer aging period of 26 days.

onto the BHJ surface. While this process did not fully restore the initial device PCE, it significantly reduced the S-shape feature in the *J–V* curve of the degraded device (Fig. 5). Since replacing the cathode suppressed the S-shape feature in degraded, high M_n PBDTTPD:$PC_{61}BM$ solar cells, the device degradation can be ascribed to an electron extraction barrier at the cathode. In an attempt to prevent this cathodic degradation, we fabricated solar cells with various interlayers and cathodes, including lithium fluoride and aluminum, calcium and silver, and cesium carbonate and aluminum. Neither the use of these alternative electrodes, nor various device preparation techniques, prevented OPV degradation in high M_n PBDTTPD devices (see ESI,† Section 3 and 4).

The role of low molecular weight organic impurities in device degradation

Considering that the S-shape degradation feature exclusively developed in solar cells fabricated from the three batches of high M_n PBDTTPD, the degradation process must have stemmed from something inherent to these polymer batches. Metal catalysts were used in Stille cross-coupling polymerization reactions and could have remained trapped within the polymer samples. We explored the possibility that metal catalyst impurities could be the source of instability in high M_n PBDTTPD by measuring the palladium content in high and low M_n polymer with inductively coupled plasma mass spectrometry (ICP-MS

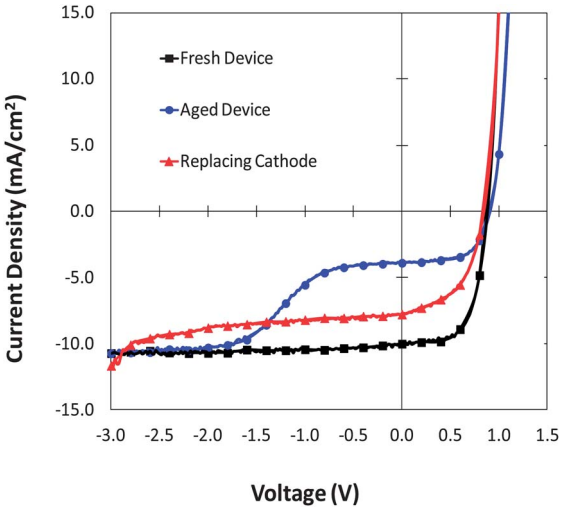

Fig. 5 The S-shape feature from a degraded, high M_n (Batch #H2) device is eliminated by removing the cathode with Scotch tape and then evaporating a new cathode.

Table 1 Palladium metal impurities measured by ICP-MS

Polymer	Palladium (ppm)
Low M_n PBDTTPD	1000
High M_n PBDTTPD	250

performed by Evans Analytical Group, Table 1). While metal content has been shown to detrimentally affect organic electronic devices,[39–41] it did not appear to cause the S-shape feature, as the palladium content was 75% lower in our high M_n PBDTTPD than in our low M_n PBDTTPD. Despite its relatively high palladium content, low M_n PBDTTPD-based devices did not form S-shape degradation features in their *J–V* curves.

Since palladium content did not appear to cause S-shape formation in high M_n PBDTTPD solar cells, we considered the role of low molecular weight organic contaminants, perhaps trapped within the high M_n PBDTTPD (and not in the low M_n PBDTTPD), on BHJ solar cell degradation. We proposed that, if present, small organic impurities might diffuse to the interface between the active layer and the cathode, causing S-shape features upon reaction with the metal cathode or interlayer.[61,62] The extent of degradation would thus depend on the amount of reacted surface area, where the severity of the S-shape degradation would increase as more small molecules reach the interface and react.

To probe for the presence of organic impurities, the size exclusion chromatograms (SEC) of the polymers were analyzed with an emphasis on the low molecular weight region (high retention times) where small molecule contaminants may be detected. The chromatograms of high and low M_n PBDTTPD did not, however, show different peaks below 2 kDa. Electrospray ionization, electron impact, and gas chromatography-mass spectrometry spectra also did not detect monomer or degradation impurities in the high and low M_n polymer samples.

We considered that low molecular weight contaminants could be present in concentrations below the detection limit of the instruments used for these analyses (see ESI,† Section 5) so we turned to an indirect approach to examine the effect of low molecular weight contaminants on solar cell stability. TPD monomer was intentionally incorporated into low M_n PBDTTPD:$PC_{61}BM$ devices. We chose the TPD monomer as our intentional contaminant because it was a low molecular weight organic component that was used in excess in the polymerization reaction of PBDTTPD. A similar experiment was used to study the effect of $PC_{84}BM$ impurities in PCDTBT:$PC_{71}BM$ BHJ and trace metal impurities in PTB7 solar cells, and the technique was found to be especially useful for assessing the role of impurities at concentrations below effective detection limits.[41,63]

Experimentally, the TPD monomer was added to solutions of low M_n PBDTTPD:$PC_{61}BM$ at 0.1 mol% and 1.0 mol% (molarity of TPD relative to the combined molarity of PBDTTPD and $PC_{61}BM$), and solar cells were fabricated using the same processing conditions as for the non-contaminated devices. Intentional TPD contamination only slightly lowered initial device performance. Control solar cells with no contaminant, solar cells with 0.1 mol% TPD, and solar cells with 1.0 mol% TPD achieved up to 5.26%, 5.12%, and 4.64% PCE, respectively (see ESI,† Section 6). However, after 21 days of glovebox storage, several of the devices contaminated with 0.1 mol% TPD developed a modest S-shape feature in the reverse bias region of their *J–V* curves (Fig. 6b). The addition of 1.0 mol% TPD resulted in significant S-shape formation in 60% of devices (Fig. 6c). The result was reproduced in 70% of devices in a second experiment where 1.0 mol% TPD was added to low M_n PBDTTPD:$PC_{61}BM$ solutions. As with solar cells fabricated from high M_n PBDTTPD, the S-shape feature characteristic of device degradation developed at approximately −1.25 V. At reverse biases exceeding −2 V, the photocurrent of the aged, contaminated devices also converged to the initial photocurrent. The same mechanism that caused high M_n PBDTTPD solar cells to degrade was likely responsible for the observed S-shape feature in TPD contaminated devices. Since the addition of 1.0 mol% TPD to solar cells more consistently reproduced the S-shape degradation feature of high M_n PBDTTPD, it is inferred that high M_n PBDTTPD polymers contained impurities at similar concentrations (see ESI,† Section 5).

We calculate that about 10^{14} to 10^{15} molecules of TPD (or a another similarly sized organic molecule) would be required to create a perfect monolayer on the surface of a solar cell substrate (2.5 cm^2), assuming the area of one TPD molecule is 0.15–0.50 nm^2 (see ESI,† Section 7). The PBDTTPD:$PC_{61}BM$:TPD films are 100 nm thick. Assuming the volume percent of each component in the film is proportional to the molar percent in solution, then 1.0 mol% TPD in solution corresponds to 2.5×10^{14} nm^3 TPD in the film. Assuming a TPD molecular volume of 0.15–0.50 nm^3, there are between 5×10^{14} and 2×10^{15} TPD molecules in a film, which matches the estimate to cover the entire substrate with a perfect monolayer. Imperfect monolayer formation, perhaps through aggregation of the small molecule impurities or incomplete access to the active layer–cathode interface, could lead to incomplete reaction with the cathode and varying extents of device degradation. An impurity concentration of 1.0 mol% could thus be sufficient to cause widespread, yet not necessarily complete, surface converage of

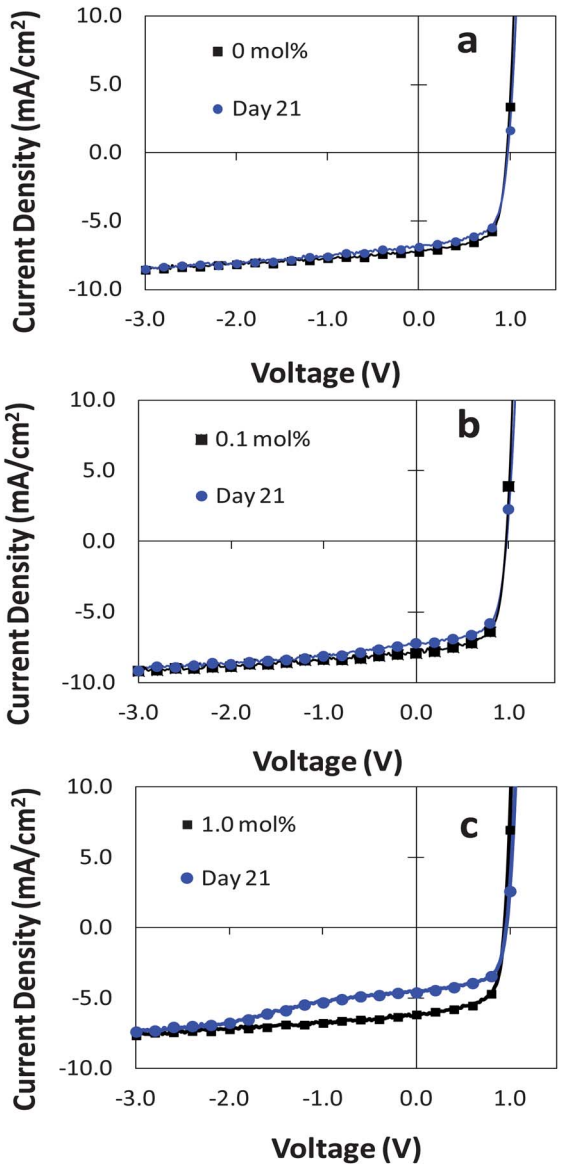

Fig. 6 Fresh and aged *J–V* curves of representative low M_n (Batch #L1) PBDTTPD:$PC_{61}BM$ devices to which TPD was intentionally added. (a) Solar cells with no intentionally added TPD show little degradation over 21 days. (b) Solar cells with 0.1 mol% TPD show a slight S-shape feature at −1.25 V after 21 days of storage. (c) Solar cells with 1.0 mol% TPD show significant S-shape formation after 21 days of aging, matching that of high M_n PBDTTPD:$PC_{61}BM$ solar cells.

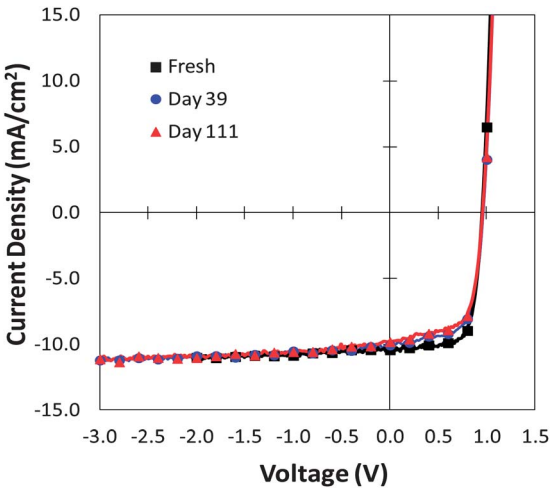

Fig. 7 Preparative SEC-treated high M_n PBDTTPD:$PC_{61}BM$ devices show less than 10% degradation of J_{SC} and no S-shape formation over 111 days of aging.

contaminant on the substrate, leading to the substantial (though not complete) observed cathode degradation.

Further polymer purification improves solar cell stability

If low molecular weight organic impurities, such as unreacted monomers, coupling byproducts, oligomers, or other degraded impurities, caused the rapid development of S-shape degradation curves in high M_n PBDTTPD BHJ solar cells, then reducing all low molecular weight content in high M_n PBDTTPD could lead to relatively stable BHJ solar cells. In addition to repeated precipitation and soxhlet extraction, a solution of high M_n PBDTTPD was further purified by preparative SEC. With this technique, the low molecular weight constituents were separated from the higher molecular weight fraction (Fig. S18 and S19†). Solar cells fabricated from this new fraction of high M_n PBDTTPD achieved a maximum PCE of 7.3% (Fig. 7), which corresponds to the efficiency obtained with soxhlet-treated high M_n PBDTTPD. More notably, the S-shape degradation feature did not develop in any of the 50 SEC-treated high M_n PBDTTPD devices after an extended 111 days aging period (Fig. 7).

Even if their structure is unknown, this result further links the S-shape degradation feature in BHJ solar cells fabricated from high M_n PBDTTPD to the presence of some type of low molecular weight contaminant in the active layer. We suspect that solvent-based purification steps alone may not have the same level of effectiveness on some high molecular weight materials, especially if a high M_n leads to a greater propensity for polymers to aggregate in solution. Finally, this result suggests a need to further purify high M_n polymers in order to reach device stabilities comparable to those of their low M_n counterparts.

Conclusions

We have shown that high M_n PBDTTPD:$PC_{61}BM$ solar cells yield initial device PCEs as high as 7.3%, but can suffer from rapid degradation characterized by the appearance of S-shaped features in the reverse bias region of *J–V* curves. BHJ solar cells fabricated from low M_n PBDTTPD are not as efficient initially but do not suffer from the same S-shape degradation feature. We have shown that intentionally introduced low molecular weight impurities structurally similar to the polymer can induce degradation in BHJ solar cells. The specific degradation feature observed in this study is suspected to be a consequence of organic contaminants accumulating at and possibly reacting with the device cathode. Although low molecular weight impurities in high M_n PBDTTPD are not directly observed by standard analytical methods, we find that solar cells fabricated from high M_n PBDTTPD, subjected to fractionation by preparative SEC, do not show S-shape degradation during glovebox storage over an extended period. We infer that solvent-based

purification approaches, such as repeated precipitations and soxhlet extraction, may not have the same level of effectiveness on high M_n polymers *versus* low M_n polymers. A greater propensity for high M_n polymer to aggregate in solution may explain the suspected difference in impurity content between the high and low M_n samples of PBDTTPD.

We conclude that polymer solar cell devices with high initial PCEs are not necessarily free of impurities, which may adversely affect device lifetime more than initial performance. The threshold concentration at which impurities start reducing device lifetime is difficult to observe directly *via* standard analytical methods, yet a non-negligible concentration of impurities may still be present. Careful removal of both organic and metal-based impurities from polymers is expected to yield notable improvements in OPV device lifetimes.

Experimental

Synthesis of low M_n PBDTTPD (26 kDa)

1,3-Dibromo-5-octyl-4*H*-thieno[3,4-*c*]pyrrole-4,6(5*H*)-dione (400.00 mg, 945 μmol), (4,8-bis((2-ethylhexyl)oxy)benzo[1,2-*b*:4,5-*b*′]-dithiophene-2,6-diyl)bis(trimethylstannane) (708.15 mg, 917 μmol) and chlorobenzene (24 mL) were combined in a 100 mL Schlenk flask and degassed with nitrogen for 25 min. Tris-(dibenzylideneacetone)dipalladium(0) (26.0 mg, 28.4 μmol) and tri(*o*-tolyl)phosphine (34.5 mg, 113 μmol) were added to the flask and the reaction mixture was stirred for 18 h at 110 °C, before a second round of catalyst and ligand were added to the flask. After another 18 h of stirring at 110 °C, strong complexing ligand *N*,*N*-diethyl-2-phenyldiazenecarbothioamide (130 mg, 587 μmol) and chloroform (20 mL) were added to the reaction mixture to remove residual catalyst. The reaction contents were stirred at 55 °C for 1 h before precipitation into methanol (500 mL). The precipitate was filtered through a Soxhlet thimble and purified *via* Soxhlet extraction for 2 h with methanol and 12 h with dichloromethane, before being collected in chlorobenzene. The chlorobenzene solution was then concentrated by evaporation, precipitated into methanol (400 mL) and filtered to yield 630 mg of a dark purple solid (94%). SEC analysis in chloroform: M_n = 26 kDa, PDI = 2.0.

Synthesis of high M_n PBDTTPD (36–41 kDa)

1,3-Dibromo-5-octyl-4*H*-thieno[3,4-*c*]pyrrole-4,6(5*H*)-dione (400.00 mg, 945 μmol), (4,8-bis((2-ethylhexyl)oxy)benzo [1,2-*b*:4,5-*b*′]dithiophene-2,6-diyl)bis(trimethylstannane) (708.15 mg, 917 μmol) and chlorobenzene (16 mL) were combined in a 100 mL Schlenk flask and degassed with nitrogen for 25 min. Tris(dibenzylideneacetone)dipalladium(0) (26.0 mg, 28.4 μmol) and tri(*o*-tolyl)phosphine (34.5 mg, 113 μmol) were added to the flask and the reaction mixture was stirred for 21 h at 110 °C, before a second round of catalyst and ligand were added to the flask. After another 18 h of stirring at 110 °C, strong complexing ligand *N*,*N*-diethyl-2-phenyldiazenecarbothioamide (130 mg, 587 μmol) and chloroform (16 mL) were added to the reaction mixture to remove residual catalyst. The reaction contents were stirred at 55 °C for 1 h before precipitation into methanol (400 mL). The precipitate was filtered through a Soxhlet thimble and purified *via* Soxhlet extraction for 2 h with methanol, 20 h with dichloromethane and was finally collected in chlorobenzene. The chlorobenzene solution was then concentrated by evaporation, precipitated into methanol (400 mL) and filtered to yield 626 mg of a dark purple solid (94%). SEC analysis in chloroform: M_n = 36 kDa, PDI = 1.9 (Batch #H1). Two other polymer batches were similarly prepared. SEC analysis in chloroform: Batch #H2: M_n = 37 kDa, PDI = 1.9; Batch #H3: M_n = 41 kDa, PDI = 1.8.

Determining molecular weight

For polymer molecular weight determination, polymer solutions (1 mg mL^{-1}) were prepared using HPLC grade chloroform. Samples were briefly heated and then allowed to return to room temperature prior to filtering through a 0.45 μm PTFE filter. Size exclusion chromatography (SEC) was performed with HPLC grade chloroform at an elution rate of at 1.0 mL min^{-1} through three PLgel Mixed-C columns. The particle size in the columns was 5 μm and the columns were maintained at room temperature. The SEC system consisted of a Waters 2695 Separation Module and a Waters 486 Tunable Absorption Detector. The apparent molecular weights and polydispersities (M_w/M_n) were determined with a calibration based on linear polystyrene standards using Millennium software from Waters.

Further purification of high M_n PBDTTPD

Conditions analogous to those employed for the preparation of the high M_n PBDTTPD were used for polymerization. The following material quantities were used for the polymerization: 1,3-dibromo-5-octyl-4*H*-thieno[3,4-*c*]pyrrole-4,6(5*H*)-dione (390.54 mg, 928 μmol), (4,8-bis((2-ethylhexyl)oxy)benzo[1,2-*b*:4,5-*b*′]-dithiophene-2,6-diyl)bis(trimethylstannane) (696.74 mg, 899 μmol), chlorobenzene (15.8 mL), tris(dibenzylideneacetone)dipalladium(0) (24.7 mg, 26.9 μmol), and tri(*o*-tolyl)phosphine (32.8 mg, 108 μmol). Post polymerization, the polymer mixture was stirred with complexing ligand *N*,*N*-diethyl-2-phenyldiazenecarbothioamide, and precipitated in methanol. The precipitate was purified *via* Soxhlet extraction for 8 h with methanol and 72 h with dichloromethane, before being collected with chlorobenzene. Upon concentration by solvent evaporation, and precipitation into methanol, 586 mg of polymer was collected (92%). As an added step in the purification protocol, the polymer (100 mg) was dissolved in HPLC grade chloroform (8 mL), passed through preparative SEC columns (see details below), and the tail fraction, containing low molecular-weight impurities, was separated from the main polymer fraction. Upon concentration by solvent evaporation, and precipitation into methanol, 61 mg of polymer was collected (61%). SEC analysis in chloroform: M_n = 35 kDa, PDI = 1.8.

For purification by preparative SEC, polymer solutions (12.5 mg mL^{-1}) were prepared with HPLC grade chloroform. The solutions were briefly heated, to induce complete polymer dissolution, and then allowed to return to room temperature, prior to filtering through a 0.45 μm PTFE filter. Purification was performed at room temperature with HPLC grade chloroform at

an elution rate of 15 mL min^{-1} through a set of two JAIGEL-4H-40 columns mounted on a LC-9130NEXT (JAI) system equipped with coupled UV-254NEXT and RI-700NEXT detectors.

Device preparation

Glass substrates patterned with ITO (15 Ω per square, Xinyan Technologies LTD) were scrubbed with dilute Extran 300 detergent, ultrasonicated in the same dilute detergent for 10 min, rinsed in de-ionized (DI) water for 5 min, then ultrasonicated in acetone and isopropyl alcohol baths for 10 min. Substrates were rinsed with DI water again, blown dry with nitrogen gas, and placed in an oven (95 °C) for 15 min to remove any residual water. Immediately before spinning, substrates were exposed to a UV-ozone plasma for 10 min. An aqueous solution of PEDOT:PSS (Clevios P VP AI 4083) was spin-cast at 4000 rpm onto the substrates and baked at 140 °C for 15 min. Substrates were then transferred into a dry nitrogen glovebox (<3 ppm O_2).

All solutions were prepared in the glovebox using PBDTTPD synthesized as above, and $PC_{61}BM$, purchased from Nano C. The active layer components were dissolved in chlorobenzene overnight at 115 °C. Shortly before spinning, a small amount (~10 to 20 μL) of chlorobenzene was added to the solutions to compensate for any evaporation overnight. Active layers were spin-cast from solutions at 115 °C. Optimized solar cells for both high and low M_n polymer use a 1 : 1.5 ratio by weight of PBDTTPD:$PC_{61}BM$, with a solution concentration of 8 mg mL^{-1} PBDTTPD. For intentional contamination experiments, 1,3-dibromo-5-octyl-4*H*-thieno[3,4-*c*]pyrrole-4,6(5*H*)-dione (TPD) was added to solutions of low M_n PBDTTPD:$PC_{61}BM$ in 0.1 mol% and 1.0 mol%, relative to the combined mass of PBDTTPD and $PC_{61}BM$. Thus, the 0.1 mol% solution contained 8.6 mg PBDTTPD, 12.9 mg $PC_{61}BM$, and 0.014 mg TPD. The 1.0 mol% solution contained 8.0 mg PBDTTPD, 11.7 mg $PC_{61}BM$, and 0.112 mg TPD. Active layers were spin-cast at 1200 rpm for 45 seconds (500 rpm s^{-1}).

Optimized devices of both high and low M_n used 7 nm of calcium and 150 nm of aluminum as the cathode (Ca purchased from Plasmaterials, 99.5% purity, Al purchased from K. J. Lesker, 99.999% purity). The metals were applied by thermal evaporation at pressures less than 10^{-6} Torr, and were evaporated directly onto the organic layer at rates <0.5 Å s^{-1}. For cathode removal, Scotch tape was applied evenly over the electrode and ripped off by hand, in the glovebox. Details about devices with other cathode materials are provided in the ESI.†

Device characterization

J–V measurements of solar cells were performed in the glovebox with a Keithley 2400 source meter and a Spectra-Physics 91160-1000 solar simulator calibrated to 1 sun, AM1.5 G with a NREL certified KG-5 filtered silicon photodiode. For lifetime testing, *J–V* curves were taken periodically on multiple devices on multiple substrates. Over the course of investigation, over 700 devices, from multiple solutions, cathode evaporations, and PBDTTPD samples were monitored. Between testing, devices were kept in the dark and stored inside the glovebox, which has a N_2 environment containing oxygen and water levels of <3 ppm.

Acknowledgements

The authors acknowledge Dr George Burkhard, Jason Bloking, and Plextronics for helpful discussions. We acknowledge the synthetic contribution of Dr Shiming Zhang in the photovoltaic polymer program at KAUST. This work was supported by the Center for Advanced Molecular Photovoltaics (CAMP) (Award no KUS-C1-015-21) made possible by the King Abdullah University of Science and Technology (KAUST). I.T.S.Q. was supported by the National Science Foundation Graduate Research Fellowship. J.A.B acknowledges additional funding from the National Defense Science and Engineering Fellowship. Additional support was provided for E.T.H. by the Fannie and John Hertz Foundation.

References

1 G. Yu, J. Gao, J. C. Hummelen, F. Wudl and A. J. Heeger, *Science*, 1995, **270**, 1789–1791.
2 B. Azzopardi, C. J. M. Emmott, A. Urbina, F. C. Krebs, J. Mutale and J. Nelson, *Energy Environ. Sci.*, 2011, **4**, 3741–3753.
3 Q. T. Zhang and J. M. Tour, *J. Am. Chem. Soc.*, 1998, **120**, 5355–5362.
4 P. M. Beaujuge and J. M. J. Fréchet, *J. Am. Chem. Soc.*, 2011, **133**, 20009–20029.
5 P.-L. T. Boudreault, A. Najari and M. Leclerc, *Chem. Mater.*, 2011, **23**, 456–469.
6 X. Li, W. C. H. Choy, L. Huo, F. Xie, W. E. I. Sha, B. Ding, X. Guo, Y. Li, J. Hou, J. You and Y. Yang, *Adv. Mater.*, 2012, **24**, 3046–3052.
7 Z. He, C. Zhong, X. Huang, W.-Y. Wong, H. Wu, L. Chen, S. Su and Y. Cao, *Adv. Mater.*, 2011, **23**, 4636–4643.
8 M. A. Green, K. Emery, Y. Hishikawa, W. Warta and E. D. Dunlop, *Prog. Photovoltaics*, 2012, **20**, 606–614.
9 Z. He, C. Zhong, S. Su, M. Xu, H. Wu and Y. Cao, *Nat. Photonics*, 2012, **6**, 591–595.
10 C. Cabanetos, A. El Labban, J. A. Bartelt, J. D. Douglas, W. R. Mateker, J. M. J. Fréchet, M. D. McGehee and P. M. Beaujuge, *J. Am. Chem. Soc.*, 2013, **135**, 4656–4659.
11 N. Grossiord, J. M. Kroon, R. Andriessen and P. W. M. Blom, *Org. Electron.*, 2012, **13**, 432–456.
12 M. Jørgensen, K. Norrman, S. A. Gevorgyan, T. Tromholt, B. Andreasen and F. C. Krebs, *Adv. Mater.*, 2012, **24**, 580–612.
13 C. H. Peters, I. T. Sachs-Quintana, J. P. Kastrop, S. Beaupré, M. Leclerc and M. D. McGehee, *Adv. Energy Mater.*, 2011, **1**, 491–494.
14 M. Koehl, M. Heck, S. Wiesmeier and J. Wirth, *Sol. Energy Mater. Sol. Cells*, 2011, **95**, 1638–1646.
15 X. Yang, J. K. J. van Duren, R. A. J. Janssen, M. A. J. Michels and J. Loos, *Macromolecules*, 2004, **37**, 2151–2158.
16 B. Conings, S. Bertho, K. Vandewal, A. Senes, J. D'Haen, J. Manca and R. A. J. Janssen, *Appl. Phys. Lett.*, 2010, **96**, 163301.
17 S. Bertho, G. Janssen, T. J. Cleij, B. Conings, W. Moons, A. Gadisa, J. D'Haen, E. Goovaerts, L. Lutsen, J. Manca and D. Vanderzande, *Sol. Energy Mater. Sol. Cells*, 2008, **92**, 753–760.

18 J. Vandenbergh, B. Conings, S. Bertho, J. Kesters, D. Spoltore, S. Esiner, J. Zhao, G. Van Assche, M. M. Wienk, W. Maes, L. Lutsen, B. VanMele, R. A. J. Janssen, J. Manca and D. J. M. Vanderzande, *Macromolecules*, 2011, **44**, 8470–8478.
19 C. H. Peters, I. T. Sachs-Quintana, W. R. Mateker, T. Heumueller, J. Rivnay, R. Noriega, Z. M. Beiley, E. T. Hoke, A. Salleo and M. D. McGehee, *Adv. Mater.*, 2012, **24**, 663–668.
20 B. J. Kim, Y. Miyamoto, B. Ma and J. M. J. Fréchet, *Adv. Funct. Mater.*, 2009, **19**, 2273–2281.
21 G. Griffini, J. D. Douglas, C. Piliego, T. W. Holcombe, S. Turri, J. M. J. Fréchet and J. L. Mynar, *Adv. Mater.*, 2011, **23**, 1660–1664.
22 H. Neugebauer, C. Brabec, J. C. Hummelen and N. S. Sariciftci, *Sol. Energy Mater. Sol. Cells*, 2000, **61**, 35–42.
23 L. Ma, X. Wang, B. Wang, J. Chen, J. Wang, K. Huang, B. Zhang, Y. Cao, Z. Han, S. Qian and S. Yao, *Chem. Phys.*, 2002, **285**, 85–94.
24 S. Chambon, A. Rivaton, J.-L. Gardette and M. Firon, *Sol. Energy Mater. Sol. Cells*, 2007, **91**, 394–398.
25 S. Chambon, A. Rivaton, J.-L. Gardette, M. Firon and L. Lutsen, *J. Polym. Sci., Part A: Polym. Chem.*, 2007, **45**, 317–331.
26 M. O. Reese, A. M. Nardes, B. L. Rupert, R. E. Larsen, D. C. Olson, M. T. Lloyd, S. E. Shaheen, D. S. Ginley, G. Rumbles and N. Kopidakis, *Adv. Funct. Mater.*, 2010, **20**, 3476–3483.
27 A. Aguirre, S. C. J. Meskers, R. A. J. Janssen and H.-J. Egelhaaf, *Org. Electron.*, 2011, **12**, 1657–1662.
28 M. Manceau, E. Bundgaard, J. E. Carlé, O. Hagemann, M. Helgesen, R. Søndergaard, M. Jørgensen and F. C. Krebs, *J. Mater. Chem.*, 2011, **21**, 4132–4141.
29 E. T. Hoke, I. T. Sachs-Quintana, M. T. Lloyd, I. Kauvar, W. R. Mateker, A. M. Nardes, C. H. Peters, N. Kopidakis and M. D. McGehee, *Adv. Energy Mater.*, 2012, **2**, 1351–1357.
30 J. A. Carr, K. S. Nalwa, R. Mahadevapuram, Y. Chen, J. Anderegg and S. Chaudhary, *ACS Appl. Mater. Interfaces*, 2012, **4**, 2831–2835.
31 K. R. Graham, J. Mei, R. Stalder, J. W. Shim, H. Cheun, F. Steffy, F. So, B. Kippelen and J. R. Reynolds, *ACS Appl. Mater. Interfaces*, 2011, **3**, 1210–1215.
32 D. Milstein and J. K. Stille, *J. Am. Chem. Soc.*, 1978, **100**, 3636–3638.
33 J. K. Stille, *Angew. Chem., Int. Ed. Engl.*, 1986, **25**, 508–524.
34 Z. Bao, W. K. Chan and L. Yu, *J. Am. Chem. Soc.*, 1995, **117**, 12426–12435.
35 B. Carsten, F. He, H. J. Son, T. Xu and L. Yu, *Chem. Rev.*, 2011, **111**, 1493–1528.
36 F. C. Krebs, B. Nyberg and M. Jørgensen, *Chem. Mater.*, 2004, **16**, 1313–1318.
37 K. Königsberger, G.-P. Chen, R. R. Wu, M. J. Girgis, K. Prasad, O. Repič and T. J. Blacklock, *Org. Process Res. Dev.*, 2003, **7**, 733–742.
38 K. T. Nielsen, K. Bechgaard and F. C. Krebs, *Macromolecules*, 2005, **38**, 658–659.
39 K. T. Nielsen, K. Bechgaard and F. C. Krebs, *Synthesis*, 2006, **10**, 1639–1644.
40 H. Spreitzer, A. Ludemann, R. Scheurich, N. Schulte, A. Busing and P. Stossel, *US Pat.*, US 2008/0113468 A1, 2008.
41 M. P. Nikiforov, B. Lai, W. Chen, S. Chen, R. D. Schaller, J. Strzalka, J. Maser and S. B. Darling, *Energy Environ. Sci.*, 2013, **6**, 1513–1520.
42 J. Zhou, Y. Zuo, X. Wan, G. Long, Q. Zhang, W. Ni, Y. Liu, Z. Li, G. He, C. Li, B. Kan, M. Li and Y. Chen, *J. Am. Chem. Soc.*, 2013, **135**, 8484–8487.
43 A. K. K. Kyaw, D. H. Wang, V. Gupta, W. L. Leong, L. Ke, G. C. Bazan and A. J. Heeger, *ACS Nano*, 2013, **7**, 4569–4577.
44 W. L. Leong, G. C. Welch, L. G. Kaake, C. J. Takacs, Y. Sun, G. C. Bazan and A. J. Heeger, *Chem. Sci.*, 2012, **3**, 2103–2109.
45 R. C. Coffin, J. Peet, J. Rogers and G. C. Bazan, *Nat. Chem.*, 2009, **1**, 657–661.
46 C. Piliego, T. W. Holcombe, J. D. Douglas, C. H. Woo, P. M. Beaujuge and J. M. J. Fréchet, *J. Am. Chem. Soc.*, 2010, **132**, 7595–7597.
47 Y. Zou, A. Najari, P. Berrouard, S. Beaupré, B. R. Aïch, Y. Tao and M. Leclerc, *J. Am. Chem. Soc.*, 2010, **132**, 5330–5331.
48 Y. Zhang, S. K. Hau, H.-L. Yip, Y. Sun, O. Acton and A. K.-Y. Jen, *Chem. Mater.*, 2010, **22**, 2696–2698.
49 B. J. Worfolk, T. C. Hauger, K. D. Harris, D. A. Rider, J. A. M. Fordyce, S. Beaupré, M. Leclerc and J. M. Buriak, *Adv. Energy Mater.*, 2012, **2**, 361–368.
50 D. Gupta, M. Bag and K. S. Narayan, *Appl. Phys. Lett.*, 2008, **92**, 093301.
51 D. Gupta, S. Mukhopadhyay and K. S. Narayan, *Sol. Energy Mater. Sol. Cells*, 2010, **94**, 1309–1313.
52 H. Jin, M. Tuomikoski, J. Hiltunen, P. Kopola, A. Maaninen and F. Pino, *J. Phys. Chem. C*, 2009, **113**, 16807–16810.
53 J. Wagner, M. Gruber, A. Wilke, Y. Tanaka, K. Topczak, A. Steindamm, U. Hörmann, A. Opitz, Y. Nakayama, H. Ishii, J. Pflaum, N. Koch and W. Brütting, *J. Appl. Phys.*, 2012, **111**, 054509.
54 V. P. Singh, R. S. Singh, B. Parthasarathy, A. Aguilera, J. Anthony and M. Payne, *Appl. Phys. Lett.*, 2005, **86**, 082106.
55 V. Djara and J. C. Bernède, *Thin Solid Films*, 2005, **493**, 273–277.
56 A. Kumar, S. Sista and Y. Yang, *J. Appl. Phys.*, 2009, **105**, 094512.
57 W. Tress, K. Leo and M. Riede, *Adv. Funct. Mater.*, 2011, **21**, 2140–2149.
58 A. Wagenpfahl, D. Rauh, M. Binder, C. Deibel and V. Dyakonov, *Phys. Rev. B: Condens. Matter Mater. Phys.*, 2010, **82**, 115306.
59 Q. Wang, Y. Luo and H. Aziz, *Appl. Phys. Lett.*, 2010, **97**, 063309.
60 E. Voroshazi, B. Verreet, A. Buri, R. Müller, D. Di Nuzzo and P. Heremans, *Org. Electron.*, 2011, **12**, 736–744.
61 A. V. Walker, T. B. Tighe, B. C. Haynie, S. Uppili, N. Winograd and D. L. Allara, *J. Phys. Chem. B*, 2005, **109**, 11263–11272.
62 G. L. Fisher, A. V. Walker, A. E. Hooper, T. B. Tighe, K. B. Bahnck, H. T. Skriba, M. D. Reinard, B. C. Haynie, R. L. Opila, N. Winograd and D. L. Allara, *J. Am. Chem. Soc.*, 2002, **124**, 5528–5541.
63 S. R. Cowan, W. L. Leong, N. Banerji, G. Dennler and A. J. Heeger, *Adv. Funct. Mater.*, 2011, **21**, 3083–3092.